Journal of the Mechanics and Physics of Solids 96 (2016) 18–28

Contents lists available at ScienceDirect

Journal of the Mechanics and Physics of Solids

journal homepage: www.elsevier.com/locate/jmps

Strain gradient plasticity analysis of elasto-plastic contact between rough surfaces

H. Song [a], E. Van der Giessen [a,*], X. Liu [b,*]

[a] Zernike Institute for Advanced Materials, University of Groningen, 9747 AG Groningen, The Netherlands
[b] State Key Laboratory of Nonlinear Mechanics, Institute of Mechanics, Chinese Academy of Sciences, Beijing 100190, PR China

ARTICLE INFO

Article history:
Received 16 May 2016
Received in revised form
4 July 2016
Accepted 6 July 2016
Available online 7 July 2016

Keywords:
Rough surface
Contact
Strain gradient plasticity
Pressure distribution

ABSTRACT

From a microscopic point of view, the real contact area between two rough surfaces is the sum of the areas of contact between facing asperities. Since the real contact area is a fraction of the nominal contact area, the real contact pressure is much higher than the nominal contact pressure, which results in plastic deformation of asperities. As plasticity is size dependent at size scales below tens of micrometers, with the general trend of smaller being harder, macroscopic plasticity is not suitable to describe plastic deformation of small asperities and thus fails to capture the real contact area and pressure accurately. Here we adopt conventional mechanism-based strain gradient plasticity (CMSGP) to analyze the contact between a rigid platen and an elasto-plastic solid with a rough surface. Flattening of a single sinusoidal asperity is analyzed first to highlight the difference between CMSGP and J_2 isotropic plasticity. For the rough surface contact, besides CMSGP, pure elastic and J_2 isotropic plasticity analysis is also carried out for comparison. In all cases, the contact area A rises linearly with the applied load, but with a different slope which implies that the mean contact pressures are different. CMSGP produces qualitative changes in the distributions of local contact pressures compared with pure elastic and J_2 isotropic plasticity analysis, furthermore, bounded by the two.

1. Introduction

The well-known Coulomb friction law states that the friction force F depends linearly on the normal load N through the friction coefficient μ: $F = \mu N$. Alternatively, Bowden and Tabor (1950) have argued from a microscopic point of view that friction can also be interpreted as $F = \tau A$, where τ is the shear strength of the contact and A is the real contact area, the latter being a small fraction of the apparent contact area A_0 because of the inevitable roughness of the surfaces. Consistency of the two types of description requires a linear dependence of the real contact area A on the normal force N. This is far from being trivial: for instance, the Hertzian elastic contact model gives a dependence of $N^{2/3}$ between a sphere and a flat. A nearly linear dependence was first obtained by Greenwood and Williamson (1966). They performed a statistical analysis of a rough surface with a distribution of asperity heights, based on the simplifying assumption that all peaks are spherical asperities with the same radius. Bush et al. (1975) generalized the Greenwood–Williamson model by incorporating paraboloidal asperities and a distribution of asperity size; yet, they still obtained a linear dependence.

* Corresponding authors.
E-mail addresses: E.van.der.Giessen@rug.nl (E. Van der Giessen), xiaomingliu@lnm.imech.ac.cn (X. Liu).

http://dx.doi.org/10.1016/j.jmps.2016.07.008
0022-5096/

The fact that the generalized Greenwood–Williamson model predicts that a linear relationship between A and N is far from being obvious, in view of the numerous underlying assumptions. Over the years, several of the simplifications have been criticized and, partially, mended. For example, the Greenwood–Williamson model assumes that the asperities deform independently, whereas in reality asperities will interact through the very fact that they are connected by a common substrate; a possible correction for this has been proposed by Ciavarella et al. (2008). A much more fundamental assumption is that the asperities respond elastically. However, since contact happens at the highest peaks or asperities, it is to be expected that the local contact stress gets so high that plasticity is initiated. Indeed, the real contact area measurements in polymeric magnetic media by Bhushan (1985) had already revealed that a significant portion of the deformation was not recovered after unloading.

Gao et al. (2006) were the first to systematically study plastic deformation in asperity contact. Based on the behavior of an elastic-perfectly plastic two-dimensional (2D) sinusoidal asperity under contact, they computed the real contact area between a rigid flat surface and a deformable rough surface (Gao and Bower, 2006). However, these studies did not provide any information about the connection between contact area and normal force for a real 3D rough surface in the presence of both asperity interaction and asperity plasticity. A conceptually straightforward attempt was made by Pei et al. (2005), who performed a large numerical study of a 3D elasto-plastic contact problem of self-affine rough surfaces. Their model intends to address all issues of the Greenwood–Williamson model. Besides predicting a linear dependence of contact area on normal load, these authors also provide the contact pressure distribution and contact patch size distribution, both of which are very important information for wear. A distinct limitation of this study, however, is the use of J_2 isotropic plasticity at all length scales, down to asperities that are inevitably single crystalline.

Moreover, at size scales below tens of micrometers, plasticity is now known to be size dependent, with the general trend of 'smaller being harder'. Size dependent plasticity at these scales has been convincingly demonstrated in torsion (Fleck et al., 1994), bending (Stolken and Evans, 1998) and microindentation experiments. In the latter, the indentation hardness decreases monotonically with increasing depth of indentation h, when h is in the range of sub-microns to microns (Nix, 1989; Ma and Clarke, 1995; Poole et al., 1996). Since classical plasticity theories, including J_2, do not include an intrinsic material length, size effects like these cannot be captured. The plasticity size effects mentioned above have been attributed to geometrically necessary dislocations (GNDs) associated with non-uniform plastic deformation in small volumes (Nye, 1953; Ashby, 1970; Gao and Huang, 2003). Strain gradient plasticity theories (e.g., Poole et al., 1996; Fleck and Hutchinson, 1993; Gao et al., 1999; Huang et al., 2000; Gurtin, 2002) have been developed to describe size dependent behavior for problems with an externally imposed strain gradient, such as bending, torsion and indentation (Fleck et al., 1994; Gao et al., 2015; Xue et al., 2002) as well as in problems where plastic gradients develop as a consequence of constrained plasticity, such as in void growth and composite materials (Liu et al., 2005; Huang et al., 2000; Bittencourt et al., 2003). As a few of these cited works already suggest, another approach to analyzing plasticity at these size scales is Discrete Dislocation Plasticity (DDP) in which plastic deformation emerges from the nucleation and motion of discrete dislocations in an elastic background. After 2D DDP simulations have confirmed the existence of size effects associated with GNDs in, e.g., bending and indentation (Cleveringa et al., 1997, 1999; Widjaja et al., 2005), this framework has been adopted to study contact and friction. Deshpande et al. (2004) analyzed the static friction strength through DDP together with a cohesive interface. Sun et al. (2012) carried out the plastic flattening of a sinusoidal asperity, while Song et al. (2015) investigated how interlocked asperities deform when the two surfaces slide relative to each other. All these studies focused on a unit process of a single asperity interacting with the facing surface, hence do not include information about the surface, such as surface roughness.

DDP simulations of a 3D rough surface are not feasible with the existing frameworks for 3D boundary-value problems. We therefore adopt a strain gradient plasticity theory in order to gain some understanding of how size dependent plasticity may modify the conclusions based on classical J_2 plasticity – such as a linear dependence of real contact area A on the normal force N. Because of its simplicity and success in fitting indentation results, we have chosen to adopt the conventional mechanism-based strain gradient theory (CMSGP) proposed by Huang et al. (2004). CMSGP is implemented through an ABAQUS user subroutine. When simplifying the contact between two rough surfaces, there are two options (Johnson, 1985). The first is to use a rigid flat surface to flatten the rough surface of a deformable solid with equivalent Young's modulus and Poisson ratio; this approach has been used in Gao and Bower (2006), Pei et al. (2005), and Sun et al. (2012). Alternatively, one could press a rigid rough surface into a deformable flat substrate, like in indentation; this is what Yin and Komvopoulos (2012) did. In the present paper, we utilize the former simplification and perform the simulation of elasto-plastic contact between a rigid flat and a rough surface. The height probability density function of the rough surface follows a Gaussian distribution, and the statistical correlation between heights at two random points on surface is also assumed to have a Gaussian distribution. These assumptions are used to treat surfaces as statistically homogeneous, i.e. the statistics are independent of location on the surface.

The remainder of this paper is organized as follows. Section 2 describes the methodology for generating the rough surface and a brief summary of the constitutive equations of CMSGP. Section 3 first presents results for the unit process of rough surface contact, namely that of a single sinusoidal asperity in contact. Subsequently, Section 4 presents the contact of a rough surface, checks the linear dependence, describes the distribution of contact pressures. Section 5 summarizes the key conclusions.

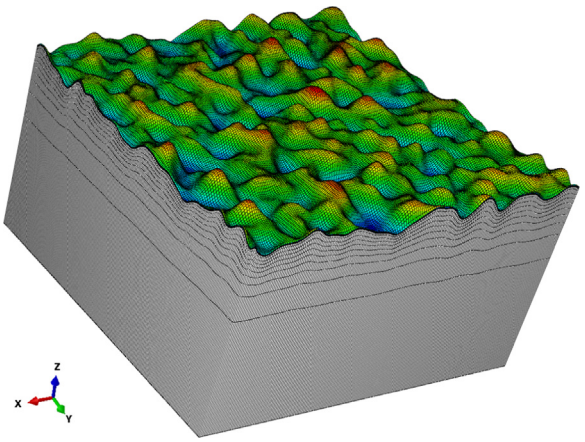

Fig. 1. Deformable solid of 10×10 μm^2 and a mean thickness of 5 μm with a representative example (rms = 0.16 μm, l_s = 0.4 μm) of a random rough surface on top. Color coding – blue: valley, red: peak. (For interpretation of the references to color in this figure caption, the reader is referred to the web version of this paper.)

2. Methodology

2.1. Rough surfaces

The simplest rough surface is one having asperities with a pre-defined size and shape, such as the rectangular and sinusoidal asperity that have been used in DDP studies by Song et al. (2015) and Dikken et al. (2015). However, these simple shapes lack the stochasticity of amplitude and wavelength that are characteristics of a real rough surface. A statistical description of a rough surface, comprising many peaks and valleys, requires information on deviations in the direction of the normal vector of the surface from its ideal form and on how the surface varies in the lateral directions. Thus, two parameters (Leach, 2013) are used to characterize a surface: the RMS height, defined as

$$\mathrm{rms} = \sqrt{\frac{\sum_{i=1}^{n}(z_i - \bar{z})^2}{n-1}}$$

and the surface correlation length l_s which describes the statistical independence of two points on a surface (Fung, 1994). For a smooth surface, $l_s = \infty$.

Random roughness with Gaussian statistics is a well-accepted approximation of many real rough surfaces (Li and Torrance, 2005). An example of a randomly rough surface generated numerically with the method of Garcia and Stoll (1984) is shown in Fig. 1. When assigning this surface profile $z_r(x, y)$ to a 3D deformable solid of height h by simply shifting only the top surface will result in heavily distorted elements. Instead, we shift all nodes in the z-direction proportionally to their initial z-position by $z_r(x_i, y_i)z_{\mathrm{ini}}/h$, such that the top surface of the solid becomes the desired rough surface while the bottom surface remains flat.

The rough solid will be pressed against a rigid flat, whose initial position is $z^{\max}$. In order for the predictions to be statistically meaningful, the surface should contain a sufficiently large number of asperities. In order to limit the computing times, however, we here compute ensemble averages of five surfaces with the same surface characteristics.

2.2. Constitutive model

The original mechanism-based strain gradient plasticity (MSGP) model was proposed by Gao et al. (1999). It is a higher-order theory, with higher-order strains and stresses plus additional boundary conditions, but was later modified into a low-order mechanism-based strain gradient plasticity theory by Huang et al. (2004). The model incorporates the effect of the strain gradient through the Taylor hardening model by explicitly decomposing the dislocation density into a density of geometrically necessary dislocations ρ_G and statistically stored dislocations ρ_S. Taylor's expression for the shear flow stress τ in terms of the dislocation density ρ then takes the form

$$\tau = \alpha\mu b\sqrt{\rho} = \alpha\mu b\sqrt{\rho_S + \rho_G}\,, \tag{1}$$

where μ is the shear modulus, b is the magnitude of the Burgers vector, and α is an empirical coefficient of the order 0.1. Within the framework of an isotropic plasticity theory, the GND density is taken to be connected to an effective plastic strain gradient η^{p},

$$\rho_G = \bar{r}\frac{\eta^{\mathrm{p}}}{b}, \tag{2}$$

where $\bar{r}$ is the Nye factor which is around 1.9 for fcc polycrystals (Arsenlis and Parks, 1999). The effective plastic strain gradient η^{p} is defined by

$$\eta^{\mathrm{p}} = \int \dot{\eta}^{\mathrm{p}} \mathrm{d}t,\ \dot{\eta}^{\mathrm{p}} = \sqrt{\frac{1}{4}\dot{\eta}^{\mathrm{p}}_{ijk}\dot{\eta}^{\mathrm{p}}_{ijk}},\ \dot{\eta}^{\mathrm{p}}_{ijk} = \dot{\varepsilon}^{\mathrm{p}}_{ik,j} + \dot{\varepsilon}^{\mathrm{p}}_{jk,i} - \dot{\varepsilon}^{\mathrm{p}}_{ij,k}, \tag{3}$$

where $\dot{\varepsilon}^{\mathrm{p}}_{ij}$ are the components of the plastic strain rate tensor and $(\,)_i$ denotes the derivative with respect to coordinate x_i.

Moreover, the tensile flow stress σ_{flow} is related to the shear flow stress τ from (1) through

$$\sigma_{\mathrm{flow}} = M\tau = M\alpha\mu b\sqrt{\rho_S + \bar{r}\eta^{\mathrm{p}}/b}, \tag{4}$$

where M is the Taylor factor, which essentially is an effective average reciprocal Schmid factor (M=3.06 for FCC polycrystals). While Eq. (4) provides a microscopic basis for σ_{flow}, macroscopically it is commonly formulated as

$$\sigma_{\mathrm{flow}} = \sigma_{\mathrm{Y}} f(\varepsilon^{\mathrm{p}}), \tag{5}$$

where ε^{p} is the effective plastic strain, σ_{Y} is the initial yield strength and the non-dimensional function f can be determined from the uniaxial stress–strain curve. Power-law hardening is described by

$$f(\varepsilon^{\mathrm{p}}) = \left(1 + \frac{E\varepsilon^{\mathrm{p}}}{\sigma_{\mathrm{Y}}}\right)^n, \tag{6}$$

where E is Young's modulus, and n is the plastic work hardening exponent ($0 \le n < 1$). In uniaxial tension, where there is no strain gradient, ρ_S can be solved from Eqs. (4)–(5),

$$\rho_S = [\sigma_{\mathrm{Y}} f(\varepsilon^{\mathrm{p}})/(M\alpha\mu b)]^2. \tag{7}$$

Gao et al. (1999) assumed that the same expression holds in the presence of strain gradients, so that substitution of Eq. (7) into Eq. (4) yields

$$\sigma_{\mathrm{flow}} = \sqrt{[\sigma_{\mathrm{Y}} f(\varepsilon^{\mathrm{p}})]^2 + M^2\bar{r}\alpha^2\mu^2 b\eta^{\mathrm{p}}} = \sigma_{\mathrm{Y}}\sqrt{f^2(\varepsilon^{\mathrm{p}}) + l\eta^{\mathrm{p}}}. \tag{8}$$

Here

$$l = M^2\bar{r}\alpha^2\left(\frac{\mu}{\sigma_{\mathrm{Y}}}\right)^2 b \approx 18\alpha^2\left(\frac{\mu}{\sigma_{\mathrm{Y}}}\right)^2 b \tag{9}$$

is the intrinsic material length which, for typical values of μ/σ_{Y}, is on the order of micrometers; for example, l = 8.65 μm in Al reinforced with SiC (Xue et al., 2002). Compared with classical plasticity theory, Eq. (8) incorporates the effect of a plastic strain gradient: under the same amount of plastic strain, smaller samples experience a higher gradient, thus have a higher flow stress which is consistent with experimental observations.

In order to avoid higher-order stress in MSGP theory, Huang et al. (2004) introduced a viscoplastic formulation which relates $\dot{\varepsilon}^{\mathrm{p}}$ directly to the effective Von Mises stress $\sigma_{\mathrm{e}} = \sqrt{3J_2}$ rather than to its rate $\dot{\sigma}_{\mathrm{e}}$ as in rate independent plasticity. Thus,

$$\dot{\varepsilon}^{\mathrm{p}} = \frac{\sigma'_{kl}\dot{\varepsilon}'_{kl}}{\sigma_{\mathrm{e}}}\left[\frac{\sigma_{\mathrm{e}}}{\sigma_{\mathrm{Y}}\sqrt{f^2(\varepsilon^{\mathrm{p}}) + l\eta^{\mathrm{p}}}}\right]^m, \tag{10}$$

with ' denoting the deviator of a second-rank tensor. A large value of the exponent m, typically ≥20, ensures that $\dot{\varepsilon}^{\mathrm{p}}$ is negligible as long as $\sigma_{\mathrm{e}} < \sigma_{\mathrm{flow}}$. Finally, the constitutive law of the resulting Conventional MSGP (CMSGP) theory can be written in a similar manner to conventional (visco-)plasticity as

$$\dot{\sigma}_{ij} = K\dot{\varepsilon}_{kk}\delta_{ij} + 2\mu\left\{\dot{\varepsilon}'_{ij} - \frac{3\sigma'_{ij}\sigma'_{kl}}{2\sigma_{\mathrm{e}}^2}\left[\frac{\sigma_{\mathrm{e}}}{\sigma_{\mathrm{Y}}\sqrt{f^2(\varepsilon^{\mathrm{p}}) + l\eta^{\mathrm{p}}}}\right]^m \dot{\varepsilon}'_{kl}\right\}, \tag{11}$$

with K being the elastic bulk modulus. Zhang et al. (2006) have extended the above infinitesimal deformation constitutive law to a hypoelastic–plastic, finite deformation theory. This is the formulation we use in the subsequent sections.

The advantage of using CMSGP is that it is a low-order theory, where the gradient of plastic strain only appears in the constitutive model, while the equilibrium equations and boundary conditions are the same as in conventional continuum theories. Thus, it can be easily implemented in finite element software for large scale contact simulations (we used ABAQUS 6.10). Moreover, the use of CMSGP avoids convergence difficulties that may appear with high-order theories such as those of Fleck and Hutchinson (1993), Gao et al. (1999) and Gurtin (2002) as a consequence of their higher-order boundary conditions. At the same time, the absence of such boundary conditions implies that CMSGP theory is unable to pick-up strain

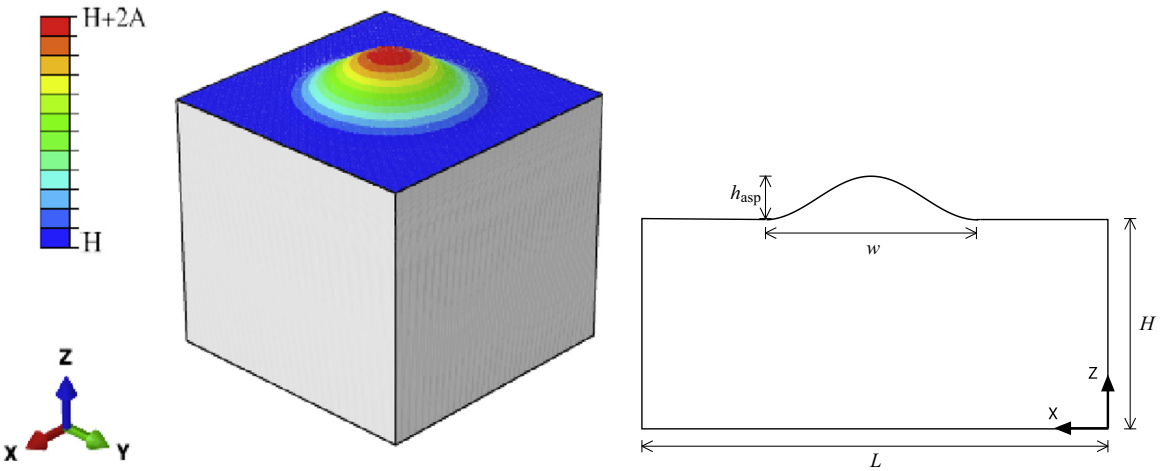

Fig. 2. (a) A 3D sinusoidal asperity is flattened by a rigid flat and (b) cross sectional profile in x–z plane of the model.

gradient effects that are induced by dislocation pile-ups against an interface or against local regions of contact in case it is not permeable for dislocations. Using discrete dislocation plasticity, Sun et al. (2012) have shown that such pile-ups play a very important role in two-dimensional flattening of an asperity when the density of dislocation multiplication sites is low. Outside this near source-controlled regime, the influence of pile-ups is unclear. As the applicability of any strain gradient plasticity for such circumstances still needs to be confirmed, we can but conclude that CMSGP results in the near-contact region will probably deviate from those of higher-order theories.

Our simulations are carried out by using the implicit solver 'ABAQUS Standard', with the CMSGP theory being implemented in subroutine UMAT. Three-dimensional eight-node linear brick (C3D8) elements are used, and the plastic strain gradients are computed at Gauss points by using the shape functions. The mesh size on the contact surface is 0.06 μm, while smaller elements (0.03 μm and 0.015 μm) were used to convince us of the lack of mesh sensitivity.

3. Flattening of a 3D sinusoidal asperity by a rigid flat

The unit model problem – compression of a single asperity from the rough surface – is shown in Fig. 2. A 3D sinusoidal asperity generated by revolution of a sinusoidal profile with amplitude $h_{asp}/2$ and wavelength w lies on top of a cuboid substrate. The elastic properties are taken to be Young's modulus $E=76$ GPa and Poisson's ratio $\nu = 0.33$, while plasticity is described by either classical J_2 theory or by the CMSGP model to see the effect of plastic strain gradient on the asperity response under contact. For J_2 with hardening, we use the properties of aluminium used in the particle size effect study of Xue et al. (2002). Their parametrization of the stress–strain curve can beconverted to the power-law hardening form of Eq. (6) with $\sigma_Y = 208$ MPa and plastic hardening exponent $n=0.136$. We start with a value of $\alpha = 0.17$ in the Taylor dislocation model which was fitted from the indentation of annealed copper (Qu et al., 2004). For the material properties mentioned above, the corresponding intrinsic length $l = 2.77$ μm.

When the asperity is flattened by prescribing the vertical displacement U of the rigid flat in the $-z$ direction, the mean contact pressure is computed from the local contact pressure $p = -\sigma_z$ by means of

$$P_m = 1/C \iint_C p(x_1, x_2)dx_1dx_2, \tag{12}$$

where C is the contact area between the rigid platen and the sinusoidal asperity. We also define a strain-like measure,

$$\varepsilon_{asp} = U/h_{asp}, \tag{13}$$

in terms of the asperity height h_{asp} and the so-called flattening distance U. As both p_m and ε_{asp} are intended to be measures of the asperity, the results should not depend on the substrate. Gao et al. (2006) have verified in a 2D model that results are independent of the substrate thickness H as long as $H > 3w$, so in our model, we use $L = H = 4w$. The bottom of the substrate is fixed, i.e. $u_1 = u_2 = u_3 = 0$, while the lateral sides are traction free. The contact between the rigid flat and the asperity is non-adhesive and frictionless.

We start out with two self-similar asperities ($h_{asp}/w = 0.2$) with $w = 2$ μm and $w = 4$ μm, respectively. Fig. 3 shows p_m–ε_{asp} curves of the two asperities with different constitutive laws: J_2 and CMSGP. We see that with J_2 plasticity, which is size independent, the two asperities exhibit nominally the same response (slight differences, especially at the start of plasticity,

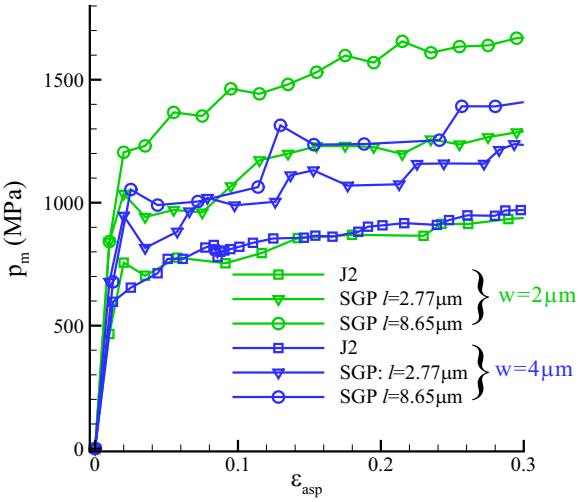

Fig. 3. Effect of size on the flattening response of self-similar asperities with $h_{asp}/w = 0.2$: mean contact pressure p_m versus asperity strain ε_{asp}. In the SGP computations, two values of the intrinsic length l are considered.

are caused by differences in the finite element mesh and automatic time increment selection by ABAQUS), whereas according to the CMSGP computation 'smaller is harder'. This can be easily understood from the fact that the flow stress in Eq. (8), i.e. $\sigma_{flow} = \sigma_{ref}\sqrt{f^2(\varepsilon^p) + l\eta^p}$, contains the plastic strain gradient η^p; as this is larger in smaller asperities, the smaller asperity is harder according to CMSPG.

Since it is the product of l and η^p that contributes to the flow stress, a larger plastic gradient η^p is, mathematically, equivalent to a larger l. Indeed, when we use $\alpha = 0.3$ as obtained from the particle size effect study (Xue et al., 2002), i.e. $l = 8.65$ μm, the size effect is even more pronounced.

Previous studies of the flattening of a 2D sinusoidal asperity (Gao et al., 2006) and of a 3D sphere (Kogut and Etsion, 2002) using J_2 theory without hardening have concluded that the mean contact pressure p_m is close to around $3\sigma_Y$ prior to complete flattening. This is confirmed for our 3D sinusoidal asperities in Fig. 4. However, with the material hardening properties used above, p_m is much larger than $3\sigma_Y$. In order to get some feeling if the contact pressure in a hardening material can be estimated by $3\sigma_{flow}$, this value is computed from (5)–(6) by using $\varepsilon^p_{asp} = \varepsilon_{asp} - (p_m/3)/E_{asp}$ as an estimate of the plastic part of the asperity strain. Here, the asperity elastic stiffness E_{asp} is defined as the initial slope of the p_m versus ε_{asp} curve (Fig. 4). The dashed curve in Fig. 4 shows that $3\sigma_{flow}$ is an upper bound to the mean contact pressure p_m. For CMSGP, σ_{flow} depends not only on the accumulated ε^p, just like in hardening J_2 solids, but also on the strain gradient. As a consequence, the average contact pressure p_m can be much higher than $3\sigma_Y$.

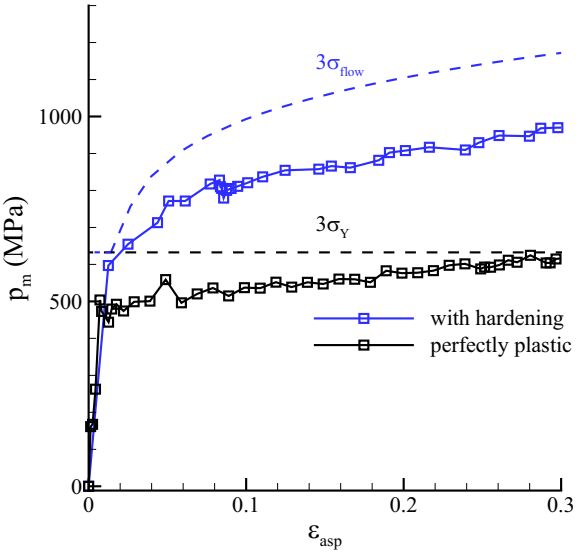

Fig. 4. Mean contact pressure p_m versus asperity strain ε_{asp} for an asperity with size $w = 4$ μm and $h_{asp} = 0.8$ μm, J_2 plasticity with hardening and without hardening.

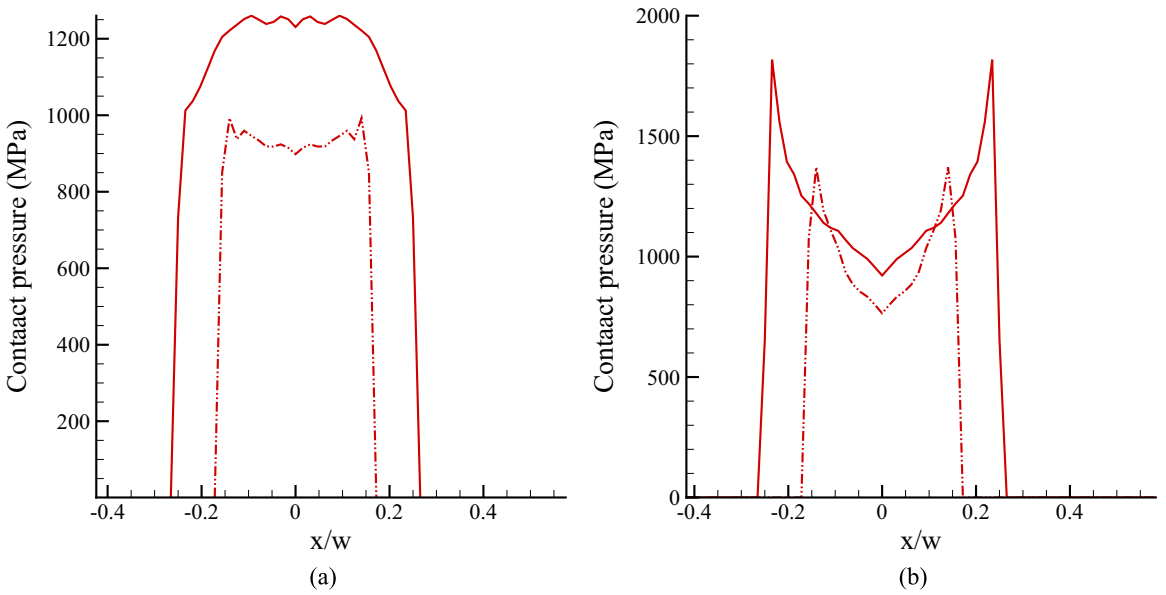

Fig. 5. Contact pressure distribution over a single asperity at different loading U (dashed lines: $U = 0.2$ μm, solid lines: $U = 0.4$ μm). (a) J_2 model and (b) SGP model with $l = 2.77$ μm.

In addition to the average contact pressure, we looked at the pressure distribution over the contact at different flattening distance U, shown in Fig. 5. It can be seen that according to J_2 hardening model, the high contact peak shifts from the edge to the center of the contact with increasing U, while in CMSGP model, the high contact pressure always appears near the edge of the contact since this is the location of the largest strain gradient. At the same U, the maximum contact pressure in CMSGP model is much higher than it is in J_2 hardening model. Thus, in a rough surface contact problem, we expect a higher probability of having larger contact pressure in CMSGP model than it in the prediction of J_2 hardening model.

4. Contact between a rigid flat and a 3D deformable rough surface

4.1. Load dependence of real contact area

The experimentally persistent linear relationship between the real contact area A and the applied load N at small loads has been verified in rough surface contact simulations in the case of pure elasticity (Hyun et al., 2004) and for J_2 plasticity (Pei et al., 2005). Here we revisit this dependence by using the CMSGP model for size dependent plasticity. The computational cell is similar to that in Fig. 1, with periodic boundary conditions in the X and Y directions. Five random realizations of random surfaces are studied for each set of material parameters and the average properties are reported.

The linear dependence still holds at small loads, shown in Fig. 6, but exhibits a slope that is in between that predicted by pure elasticity and J_2 plasticity. As the reciprocal of the slope in Fig. 6 is the real mean contact pressure N/A, the real mean contact pressure predicted by CMSGP model is higher than it is in J_2 model and smaller than it is in pure elastic model, and the difference depends on the value of the intrinsic length parameter.

4.2. Statistics of the contact pressure

Several theoretical studies (e.g., Pei et al., 2005; Hyun et al., 2004) have analyzed the statistics of the pressure distribution on the rough surface for a certain value of A/A_0, even though this quantity is difficult to assess experimentally. Since the flattening distance U is a convenient measure both in theoretical and in experimental studies, and is tightly related to A/A_0, we prefer to study the contact pressure distribution for different models ata fixed value of U. Indeed, Fig. 7(a) shows that the contact pressure distribution on five random surfaces as predicted by J_2 plasticity theory is rather insensitive to whether the distributions are computed at the same fattening distance $U = 0.25$ μm (when A/A_0 is found to be 0.3) or at the same contact area $A/A_0 = 0.1$ (which requires flattening to $U = 0.16$ μm). Moreover, in case of a linear elastic material the pressure distribution at relatively low A/A_0 scales with the total load. Hence the shape of the probability distribution is essentially unique, and we can non-dimensionalize the contact pressure distribution by normalization of the contact pressure by a convenient stress measure.

After normalization of the contact pressures predicted by pure elasticity with the yield strength of the material, Fig. 7 (b) shows that the pressure on almost all contact spots is so high that almost all asperities would have deformed

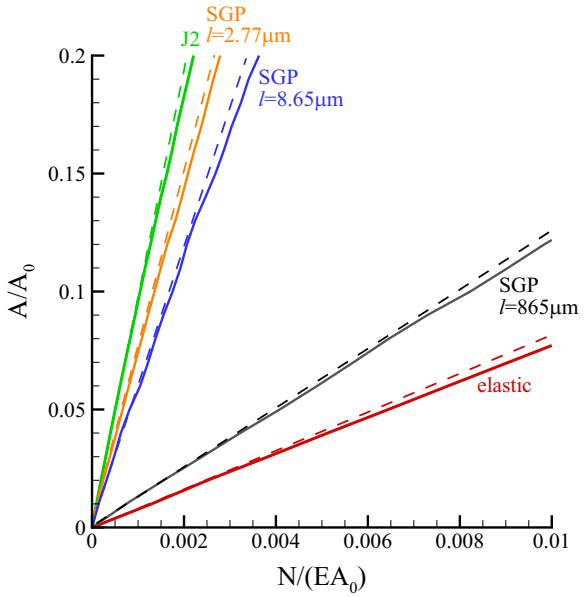

Fig. 6. Linear dependence of the real contact area on the applied normal load. The dashed lines are linear fits to the behavior at small areas.

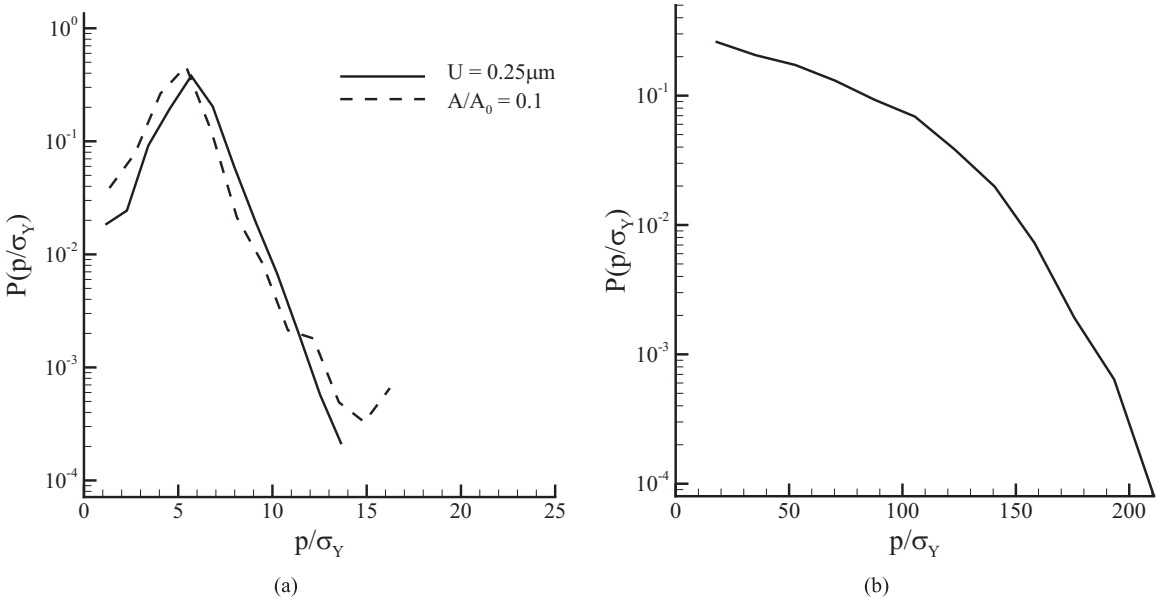

Fig. 7. Probability distribution of the local contact pressures on five random rough surface characterized by rms = 0.08 μm and correlation length l_s = 0.4 μm. (a) Prediction by J_2 theory with σ_Y = 208 MPa and n=0.136 for a prescribed flattening distance U = 0.25 μm and at the load where A/A_0 = 0.1. (b) Distribution of contact pressures on an elastic material at U = 0.25 μm, normalized by σ_Y = 208 MPa.

permanently if plasticity were possible. When plasticity is taken into account – either size independent or size dependent – the mean contact pressure is much lower, and the contact pressure displays a totally different distribution compared with pure elastic model, see Fig. 8. Instead of a monotonically decaying distribution, there is a distinct peak in the distribution. When size dependent plasticity is considered, the distribution shifts to higher values, i.e. contact pressure becomes larger when plastic deformation is size dependent.

The pressure distribution also depends on the surface roughness parameters. Fig. 9a shows the comparison of probability distribution of contact pressure when the rms of the surface changes from 0.04 μm to 0.16 μm at the same correlation length l_s = 0.4 μm. The difference in the predictions by J_2 and CMSGP is seen to increase with increasing roughness. For J_2 size independent plasticity, the peak of the distribution is more or less the same, as already observed in Pei et al. (2005), while the distribution widens. However, the change in distribution according to the size dependent plasticity model CMSGP is much more significant: not only the probability of larger contact pressure is higher, but also the peak of the distribution

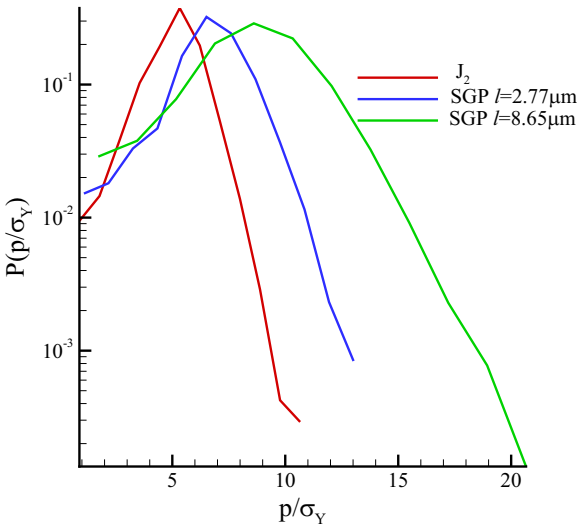

Fig. 8. Probability distribution of the local contact pressure at $U = 0.25\ \mu m$ on a rough elasto-plastic material with rms = 0.08 μm and $l_s = 0.4\ \mu m$.

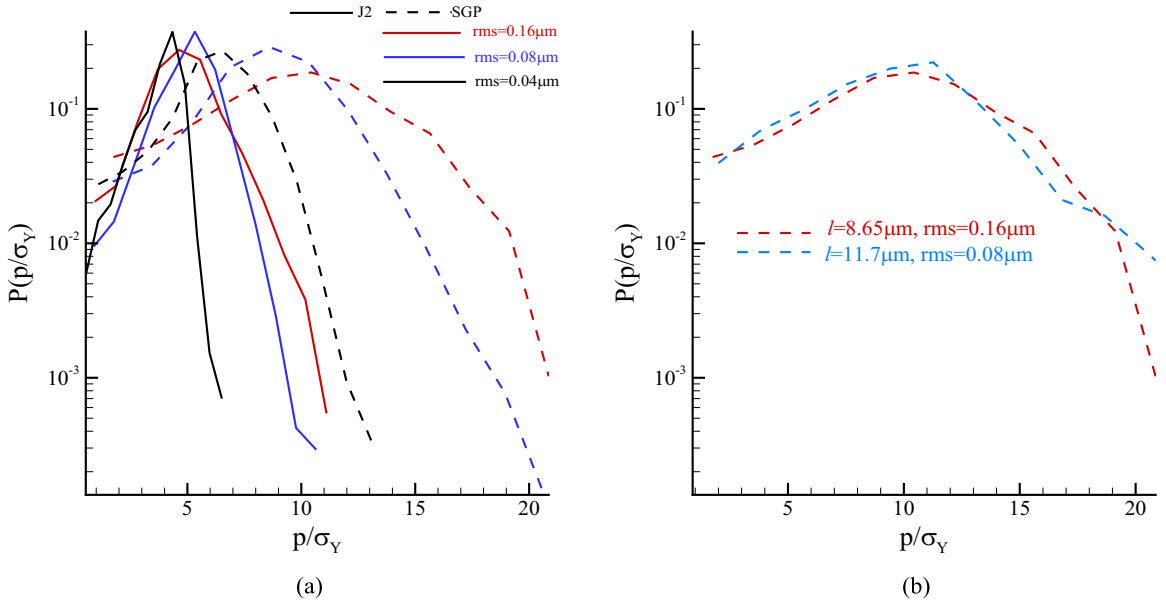

Fig. 9. Probability distribution of the local contact pressure at $U = 0.25\ \mu m$ normalized by the material yield strength in elasto-plastic model: (a) for surfaces with different rms (0.04 μm, 0.08 μm, 0.16 μm), when the intrinsic material length scale in the CMSGP model is $l = 8.65\ \mu m$; (b) comparison between {$l = 11.7\ \mu m$, rms = 0.08 μm} and {$l = 8.65\ \mu m$, rms = 0.16 μm}.

shifts to higher value. The reason is that when plasticity is size dependent, a rougher surface has sharper contact asperities which introduce larger strain gradients resulting in higher contact pressures.

As noted in the single asperity study in Section 3, a higher plastic gradient η^p is mathematically equivalent to a larger l in CMSGP model. Hence, increasing the surface roughness is equivalent to assigning a larger l while keeping the roughness the same. This is confirmed in Fig. 9b: the pressure distribution for $l = 11.7\ \mu m$ and rms = 0.08 μm is similar to that with $l = 8.65\ \mu m$ and rms = 0.16 μm.

The sensitivity of the pressure distribution to the material model used is biased by the fact that the overall pressure also depends on the model. In order to remove this bias, we now plot the probability distribution of the contact pressure p normalized by the mean of contact pressure $\langle p \rangle$. Using different values of the material intrinsic length l in the CMSGP theory, Fig. 10 clearly shows the transition from size independent plastic behavior to elastic behavior. We see that when the strain gradient effect is small, for example when $l = 2.77\ \mu m$, the SGP prediction of $p/\langle p \rangle$ coincides more or less with that of size independent J_2 theory, even though the mean contact pressures $\langle p \rangle$ are quite different, see Fig. 8. The $p/\langle p \rangle$ distributions having the same shape suggests that the strain gradient effect is equivalent to increasing the material yield stress in size independent plasticity model. However, as the strain gradient effect gets more dominant, the distribution becomes wider

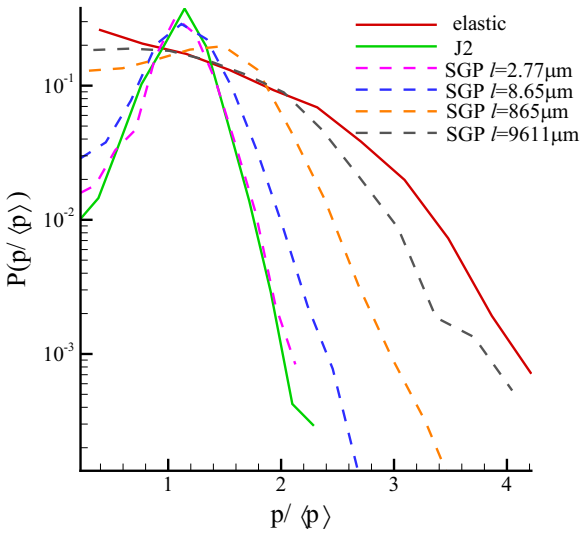

Fig. 10. Probability distribution of $p/\langle p\rangle$ on a rough surface (rms = 0.08 μm, l_s = 0.4 μm) according to J_2 model, CMSGP with different intrinsic lengths and a purely elastic model.

and therefore this equivalence no longer applies. In the large gradient limit, the distribution becomes almost the same as with a purely elastic model.

5. Summary and conclusion

In this paper, we have adopted CMSGP theory to analyze the elasto-plastic contact between a rigid platen and an elasto-plastic solid with a rough surface and have contrasted the results to predictions by pure elasticity and by J_2 plasticity.

The strain gradient induced during flattening of an asperity gives rise to a higher flow stress in the CMSGP model, so that the average contact pressure is higher than it is according to size independent J_2 plasticity. Also, the distribution of the pressure over the contact area is different: the highest contact pressure always occurs around the edge of the contact in the CMSGP model, whereas according to J_2 model, the peak shifts from the edge to the center with increasing load.

When a rough surface is flattened, the contact area increases nearly linearly with the load for all material models considered. The mean contact pressures N/A, however, are very different, with the prediction by CMSGP being in between those of pure elasticity and J_2 plasticity.

If the solid responds in an elastic manner, the local contact pressures can be much higher than the material yield strength σ_Y. When plastic deformation is possible, these high pressures are reduced to lower value, thus giving rise to a peak in the distribution. The position of this peak is correlated to σ_Y, as discussed by Pei et al. (2005). When size dependence of plasticity is included, the overall distribution shifts to higher pressure levels (Fig. 8), as if σ_Y were increased for size independent plasticity. However, this equivalence is not always true (Fig. 10): when the strain gradient effect is more pronounced (larger l), the probability distribution of contact pressures normalized by the mean pressure widens and becomes more similar to the distribution for pure elasticity.

Size dependent plasticity magnifies the sensitivity of contact pressure to the surface roughness (Fig. 9a): a larger surface roughness gives rise to a bigger difference between size independent and size dependent plasticity. As surface roughness not only changes the contact morphology, but also influences the strain gradient, it affects the effective plastic flow stress in size dependent plasticity. Increasing the surface roughness results in a larger strain gradient, which is mathematically equivalent to having a larger material intrinsic length l in CMSGP theory (Fig. 9b).

Throughout this paper, plasticity significantly reduces the contact pressure, both the magnitude of the pressure and the range of the distribution. Moreover, depending on the magnitude of the plastic strain gradient which is larger for a rougher surface, size dependent plasticity gives quantitatively different results with size independent J_2 theory. It bridges the predictions of pure elasticity and J_2 plasticity (Fig. 10).

This fundamental study of elasto-plastic contact problem highlights the importance of size dependent plasticity for friction related studies. Extension of the present work to typical friction studies such as shear of contacting surfaces, and surface ploughing seem interesting avenues for future research.

Acknowledgment

The work of H.S. was supported by Foundation for Fundamental Research on Matter (FOM), which is part of the Netherlands Organisation for Scientific Research (NWO), grant no. 13POF07-1. The work of X.L. was supported by the National Basic Research Program of China through 2012CB937500, and by the National Natural Science Foundation of China (Grant no. 11202214, no. 91216108, no. 11572329), by State Key Laboratory of Mechanics and Control of Mechanical Structures (NUAA Grant no. MCMS-0114G01), by State Key Laboratory of Structural Analysis for Industrial Equipment (DUT Grant no. GZ15116).

References

Arsenlis, A., Parks, D.M., 1999. Crystallographic aspects of geometrically-necessary and statistically-stored dislocation density. Acta Mater. 47, 1597–1611.
Ashby, M.F., 1970. The deformation of plastically non-homogeneous alloys. Philos. Mag. 21, 399–424.
Bittencourt, E., Needleman, A., Gurtin, M.E., Van der Giessen, E., 2003. A comparison of nonlocal continuum and discrete dislocation plasticity predictions. J. Mech. Phys. Solids 51, 281.
Bhushan, B., 1985. The real area of contact in polymeric magnetic media. 2. Experimental data and analysis. ASLE Trans. 28.2, 181–197.
Bowden, F.P., Tabor, D., 1950. The Friction and Lubrication of Solids, Part I. Clarendon Press, Oxford, UK (Chapter 5).
Bush, A.W., Gibson, R.D., Thomas, T.R., 1975. The elastic contact of a rough surface. Wear 35, 87–111.
Ciavarella, M., Greenwood, J.A., Paggi, M., 2008. Inclusion of "interaction" in the Greenwood and Williamson contact theory. Wear 265, 729–734.
Cleveringa, H.H.M., Van der Giessen, E., Needleman, A., 1997. Comparison of discrete dislocation and continuum plasticity predictions for a composite material. Acta Mater. 45, 3163–3179.
Cleveringa, H.H.M., Van der Giessen, E., Needleman, A., 1999. A discrete dislocation analysis of bending. Int. J. Plast. 15, 837–868.
Deshpande, V.S., Needleman, A., Van der Giessen, E., 2004. Discrete dislocation plasticity analysis of static friction. Acta Mater. 52, 135–3149.
Dikken, R.J., Van der Giessen, E., Nicola, L., 2015. Plastic shear response of a single asperity: a discrete dislocation plasticity analysis. Philos. Mag. 95 (34), 3845–3858.
Fleck, N.A., Hutchinson, J.W., 1993. A phenomenological theory for strain gradient plasticity. J. Mech. Phys. Solids 41, 1825–1857.
Fleck, N.A., Muller, G.M., Ashby, M.F., Hutchinson, J.W., 1994. Strain gradient plasticity theory and experiment. Acta Metall. Mater. 42, 475–487.
Fung, A.K., 1994. Microwave Scattering and Emission Models and their Applications. Artech House, Norwood (MA 02062), ISBN 0890065233, 9780890065235.
Gao, H., Huang, Y., Nix, W.D., Hutchinson, J.W., 1999. Mechanism-based strain gradient plasticity—I. Theory. J. Mech. Phys. Solids 47, 1239–1263.
Gao, H., Huang, Y., 2003. Geometrically necessary dislocation and size dependent plasticity. Scr. Mater. 48, 113–118.
Gao, Y.F., Bower, A.F., Kim, K.-S., Lev, L., Cheng, Y.T., 2006. The behavior of an elastic-perfectly plastic sinusoidal surface under contact loading. Wear 261, 145–154.
Gao, Y.F., Bower, A.F., 2006. Elastic–plastic contact of a rough surface with Weierstrass profile. Proc. R. Soc. Lond. A 462 (2006), 319–348.
Gao, Y.F., Larson, B.C., Lee, J.H., Nicola, K., Tischler, J.Z., Pharr, G.M., 2015. Lattice rotation patterns and strain gradient effects in FCC single crystals under spherical indentation. J. Appl. Mech. 82, 061007.
Garcia, N., Stoll, E., 1984. Monte Carlo calculation of electromagnetic-wave scattering from random rough surfaces. Phys. Rev. Lett. 52, 1798–1801.
Greenwood, J.A., Williamson, J.B.P., 1966. Contact of nominally flat surfaces. Proc. R. Soc. Lond. A 295 (1442), 300–319.
Gurtin, M.E., 2002. A gradient theory of single-crystal viscoplasticity that accounts for geometrically necessary dislocations. J. Mech. Phys. Solids 50, 5–32.
Huang, Y., Gao, H., Nix, W.D., Hutchinson, J.W., 2000. Mechanism-based strain gradient plasticity—II. Analysis. J. Mech. Phys. Solids 48, 99–128.
Huang, Y., Qu, S., Hwang, K.C., Li, M., Gao, H., 2004. A conventional theory of mechanism-based strain gradient plasticity. Int. J. Plast. 20, 753–782.
Hyun, S., Pei, L., Molinari, J.F., Robbins, M.O., 2004. Finite-element analysis of contact between elastic self-affine surfaces. Phys. Rev. E 70, 026117.
Johnson, K.L., 1985. Contact Mechanics. Cambridge University Press, Cambridge, UK (Chapter 2).
Kogut, L., Etsion, I., 2002. Elastic–plastic contact analysis of a sphere and a rigid flat. J. Appl. Mech. 69, 657–662.
Leach, R., 2013. Characterisation of Areal Surface Texture. Springer, Berlin, ISBN 9783642364570.
Li, H., Torrance, K.E., 2005. An experimental study of the correlation between surface roughness and light scattering for rough metallic surfaces. In: Proceedings of SPIE, vol. 5878.
Liu, B., Huang, Y., Li, M., Hwang, K.C., Liu, C., 2005. A study of the void size effect based on the Taylor dislocation model. Int. J. Plast. 21, 2107–2122.
Ma, Q., Clarke, D.R., 1995. Size dependent hardness of silver single crystal. J. Mater. Res. 10, 853–863.
Nix, W.D., 1989. Mechanical properties of thin films. Mater. Trans. 20A, 2217–2245.
Nye, L., 1953. Some geometrical relations in dislocated crystals. Acta Metall. Mater. 1, 153–162.
Pei, L., Hyun, S., Molinari, J.F., Robbins, M.O., 2005. Finite element modeling of elasto-plastic contact between rough surfaces. J. Mech. Phys. Solids 53 (11), 2385–2409.
Poole, W.J., Ashby, M.F., Fleck, N.A., 1996. Micro-hardness of annealed and work-hardened copper polycrystals. Scr. Mater. 34, 559–564.
Qu, S., Huang, Y., Nix, W.D., Jiang, H., Zhang, F., Hwang, K.C., 2004. Indenter tip radius effect on the Nix–Gao relation in micro- and nanoindentation hardness experiments. J. Mater. Res. 19, 3423–3434.
Song, H., Dikken, R.J., Nicola, L., Van der Giessen, E., 2015. Plastic ploughing of a sinusoidal asperity on a rough surface. J. Appl. Mech. 82 (7), 071006.
Stolken, J.S., Evans, A.G., 1998. A microbend test method for measuring the plasticity length scale. Acta Mater. 46, 5109–5115.
Sun, F., Van der Giessen, E., Nicola, L., 2012. Plastic flattening of a sinusoidal metal surface: a discrete dislocation plasticity study. Wear 296, 672–680.
Widjaja, A., Van der Giessen, E., Needleman, A., 2005. Discrete dislocation modelling of submicron indentation. Mater. Sci. Eng. A 400–401, 456–459.
Xue, Z., Huang, Y., Li, M., 2002. Particle size effect in metallic materials: a study by the theory of mechanism-based strain gradient plasticity. Acta Mater. 50, 149–160.
Yin, X., Komvopoulos, K., 2012. A discrete dislocation plasticity analysis of a single-crystal semi-infinite medium indented by a rigid surface exhibiting multi-scale roughness. Philos. Mag. 92 (24), 2984–3005.
Zhang, F., Huang, Y., Hwang, K.C., 2006. The indenter tip radius effect in micro- and nanoindentation hardness experiments. Acta Mech. Sin. 22, 1–8.